JOURNAL OF SOLID STATE CHEMISTRY 94, 260–273 (1991)

Lithium Aluminate-Doped Lithium Orthosilicate: Sol–Gel Ceramics and Lithium Dynamics

M. SMAIHI, D. PETIT, J. P. KORB, AND J. P. BOILOT

Groupe de Chimie du Solide, Laboratoire de Physique de la Matière Condensée, Ecole Polytechnique, 91128 Palaiseau Cedex, France

Received February 7, 1991

Dense ceramics ($Li_{4+x}Si_{1-x}Al_xO_4$ with $0 \leq x \leq 0.3$) are obtained by sintering at 700–900°C, without prior calcination, of sol-gel powders prepared by an alkoxide–hydroxide route. In comparison with the pure lithium orthosilicate (3×10^{-4} S · cm^{-1} at 350°C), only a slight enhancement of the ionic conductivity is noted for monophase ceramics with Li_4SiO_4-type structure (5×10^{-4} S · cm^{-1} at 350°C for $x = 0.3$). Higher conductivity (2×10^{-2} S · cm^{-1} at 350°C) is observed for an heterogeneous material formed of a lithium silicoaluminate phase ($x = 0.2$) with the Li_4SiO_4-type structure coexisting with lithium hydroxide. In this two-phase material, ac conductivity and ^{7}Li spin-lattice relaxation data are consistent with the formation of a new kinetic path, via a thin layer along the interface, which enhances the lithium mobility. © 1991 Academic Press, Inc.

Introduction

Interest has been shown in systems based on lithium orthosilicate (Li_4SiO_4) which have potential applications both as solid electrolytes in solid state devices (*1*) and as breeder materials for fusion reactors (*2*). High Li^+ ion conductivities have been observed in systems having the Li_4SiO_4-type structure. This structure is formed of isolated $(SiO_4)^{4-}$ anionic clusters with ordered distribution of Li^+ ions over available cationic sites in a monoclinic unit cell ($P2_1/m$ space group) (*3*). The introduction of mobile ion vacancies in the lithium sites by doping sharply enhances the ionic conductivity as noted in the Li_4SiO_4–Li_3PO_4 solid solution (*4–6*). The highest conductivity has been found at 40 mol% Li_3PO_4 (10^{-2} S · cm^{-1} at 300°C) with a low activation energy (0.55 eV) (*4*). Moreover, it seems that a very slightly lower conductivity can be obtained with silicoaluminates compounds (*5, 7*).

In fact, in the system Li_2O–Al_2O_3–SiO_2, Jackowska *et al.* (*7*) have shown that Li_4SiO_4 forms two limited ranges of solid solutions:

—$Li_{4+x}Si_{1-x}Al_xO_4$ with $0 \leq x \leq 0.4$ on the interface of Li_4SiO_4–Li_5AlO_4. The replacement mechanism is $Si^{4+} \rightarrow Al^{3+} + Li^+$. Hence, the Al^{3+} ions occupy Si^{4+} sites and the extra lithium ions must occupy interstitial sites.

—$Li_{4-3y}Al_ySiO_4$ with $0 \leq y \leq 0.06$ on the interface of Li_4SiO_4–$LiAlSiO_4$. The replacement mechanism is $3Li^+ \rightarrow Al^{3+}$. Hence, the Al^{3+} ions occupy Li^+ sites and additional Li^+ vacancies are created.

In comparison with the pure Li_4SiO_4 (3×10^{-4} S · cm^{-1} at 350°C), in both solid solutions, and especially in the first, a large increase in conductivity seems to occur.

0022-4596/91 $3.00

Copyright © 1991 by Academic Press, Inc.
All rights of reproduction in any form reserved.

TABLE I

PREPARATION AND CONDUCTIVITY DATA FOR CONVENTIONAL CERAMICS IN THE Li_4SiO_4–Li_5AlO_4 SOLID SOLUTION ($Li_{4+x}Si_{1-x}Al_xO_4$).

Compound	Ceramic processing	Conductivity measurements	Results σ ($S \cdot cm^{-1}$)	E_a (eV)
x = 0.2–0.4 (Ref. (5))	$LiOH \cdot H_2O$ + SiO_2 + $Al(OH)_3$ 16 hr 850°C 12% porosity	Li electrodes monofrequency 10^4 Hz up to 250°C	10^{-3} (200°C)	0.5
x = 0.3–0.4 (Ref. (7))	[a] Li_2CO_3 + SiO_2 + Al_2O_3 900°C 20–30% porosity	Gold electrodes 5×10^2–5×10^4 Hz up to 500°C	10^{-4} (200°C) 5×10^{-3} (400°C)	0.5

[a] The samples are crushed and refired several times.

Table I summarizes previous conductivity data for $Li_{4+x}Si_{1-x}Al_xO_4$ compositions prepared by a conventional ceramic technique.

This paper first reports the preparation of sol–gel powders in the Li_4SiO_4–Li_5AlO_4 solid solution ($Li_{4+x}Si_{1-x}Al_xO_4$ with $0 \leq x \leq 0.3$) by an alkoxide–hydroxide route. Dense ceramics have been prepared by sintering at 700–900°C without prior calcination. We mainly show that the presence of molecular associations in the aluminum precursor directly influence the chemical homogeneity of the sol–gel ceramics:

—An aluminum alkoxide with a low polymerization degree leads to monophase ceramics with a lithium orthosilicate-type structure.

—An aluminum alkoxide highly polymerized leads to diphased materials formed of a mixture of lithium silicoaluminate and lithium hydroxide phases.

Second, the lithium dynamics have been investigated by a complex impedance technique and ^7Li nuclear magnetic resonance for these two types of ceramics.

In comparison with the pure lithium orthosilicate, the ionic conductivity is not drastically enhanced in monophase ceramics. Diphasic ceramics, with lithium hydroxide located within grain boundaries, are required to observe the previously reported higher conductivity data of conventional ceramics.

Concerning ^7Li longitudinal relaxation measurements, the difference observed between two types of materials is interpreted in terms of variations of the apparent polarizability of the tetrahedra skeleton. However, the difference of the lithium mobility is relatively weak between the two materials and cannot explain the drastic change of conductivity. This shows that the enhancement of the conductivity in diphasic ceramics is due to a new kinetic path along the interface between the two phases.

Preparation of Samples

Powders of $Li_{4+x}Si_{1-x}Al_xO_4$ ($0 \leq x \leq 0.3$) have been prepared from the sol–gel method. In a first step, an ethanolic solution of tetraethoxysilane (TEOS) is hydrolyzed by slow addition of a pH 2.5 HNO_3 + water mixture. The water/TEOS (H) and EtOH/TEOS (A) molar ratios are respectively fixed to 1 and 4. After 1 hr, a second solution containing aluminum *sec*-butoxide in buta-

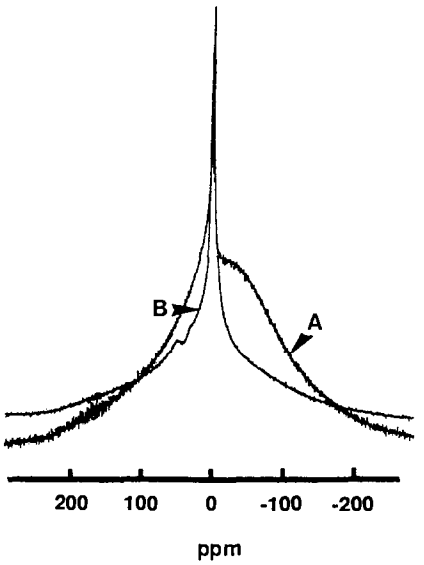

FIG. 1. ^{27}Al NMR spectra recorded at 93.8 MHz for two commercial aluminum *sec*-butoxides ($Al(H_2O)_6^{3+}$ used as the ^{27}Al chemical shift reference): A, from Alfa-Products (95 wt%) and B, from Aldrich (97 wt%).

nol (0.6 mol/liter) is mixed into the prehydrolyzed TEOS solution. Then, after 15 min, an aqueous suspension of $LiOH,H_2O$ (30 mol · liter^{-1}), heated at 60°C, is added, with vigorous stirring, into the previous optically clear mixture. For each composition, the solution rapidly leads to the formation of a white sol which is oven dried for 3 hr at 150°C in a CO_2-free atmosphere. Concerning the aluminum alkoxide, two different commercial *sec*-butoxides are used. The two solutions, in butanol, are characterized by ^{27}Al NMR spectra recorded at 93.8 MHz ($Al(H_2O)_6^{3+}$ used as the ^{27}Al chemical shift reference):

—The first, from Alfa-Products (95 wt%), is viscous and its NMR spectrum presents a very broad line (Fig. 1). This indicates a high degree of polymerization for this alkoxide and probably a low chemical reactivity. Silicoaluminate powders ($x = 0.1, 0.2$, and 0.3), prepared from this precursor, are hereafter called A.

—The second, from Aldrich (97 wt%), is more liquid and its NMR spectrum exhibits intense sharp peak at 3 ppm and a weakly intense peak at 60 ppm (Fig. 1). This shows a lower degree of polymerization for this alkoxide and obviously higher chemical reactivity. Silicoaluminate powders ($x = 0.2$ and 0.3), prepared from this precursor, are hereafter called B.

X-ray diffraction patterns from dried silicoaluminate powders (Cu$K\alpha$ radiation) exhibit small peaks corresponding to the LiOH phase for the B-type and to the $LiOH,H_2O$ phase for the A-type. The lithium orthosilicate-type phase is well crystallized at 700°C for the two types of powders, with a small amount of lithium carbonate which disappears at 800°C. Figure 2 shows thermal analysis curves (TGA and DTA heating rate, 300°C/hr) for a B dried powder ($x = 0.3$). After heating at 800°C, a weight loss of 20% is deduced from the TGA curve. On the DTA curve, three endothermic peaks corresponding to the removal of water (100°C), the decomposition of the lithium hydroxide (422°C) and of the lithium carbonate (710°C), are observed. This latter phase is formed during the combustion of the organic groups (broader exothermic peak at 320–360°C).

The specific surface areas, measured by the BET method, are of 100 and 150 m^2/g for the A and B dried powders, respectively,

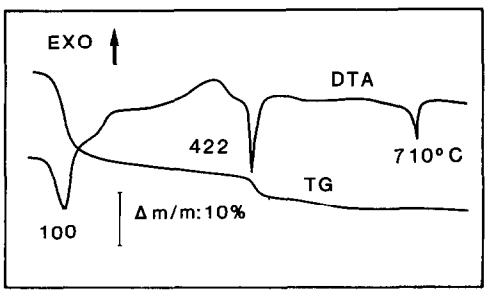

FIG. 2. Differential thermal analysis (DTA) and thermogravimetric (TGA) curves (heating rate 300°C/hr) for a B-type silicoaluminate powder ($x = 0.3$).

and decrease down to 2–3 m^2/g after heating at 600°C. Dried powders are isostatically cold-pressed into pellets under 200 MPa. The pellets are then heated at 400°C (5 hr) and sintered (7 hr) at different temperatures (700–900°C) in alumina crucibles (heating rate 100°C/hr). The samples are buried in powder of the same composition to reduce some stoichiometry variations. The sintering takes place between 600 and 750°C for B samples and in a larger temperature range for A samples (400–800°C). The densification factor, measured by the Archimedes' method, did not significantly vary (0.90–0.92) with the type of powder and with the sintering temperature in the 700–900°C range.

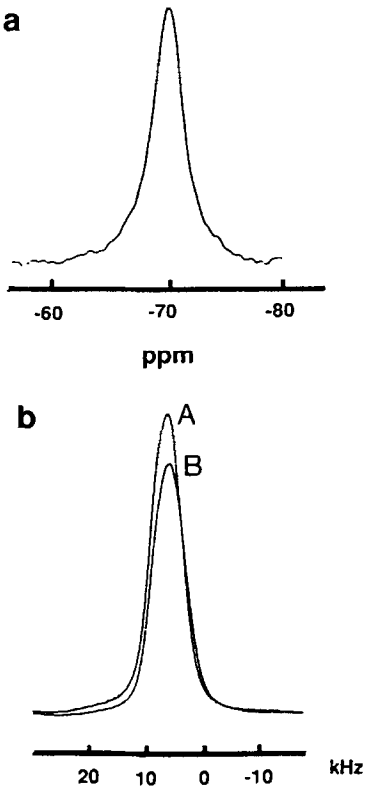

FIG. 3. NMR spectra at room temperature from silicoaluminate samples ($x = 0.2$) fired at 800°C: (a) ^{29}Si MAS-NMR spectra recorded at 71.5 MHz for A-type sample. (b) ^{27}Al static NMR spectra at 93.8 MHz for A- and B-type samples.

Structural Characterization

1. X-Ray Diffraction

In the composition range $0 \leq x \leq 0.3$, the two types of samples exhibited the same X-ray diffraction pattern, corresponding to the monoclinic lithium orthosilicate-type structure. As previously observed in the Li_4SiO_4–Li_5AlO_4 solid solution (*5*), upon substitution of Al for Si and introduction of extra lithium ions, the cell volume continuously increases (from 166 $Å^3$ to 170 $Å^3$ by increasing from 0 to 0.3).

2. ^{29}Si and ^{27}Al Nuclear Magnetic Resonance

Crystal structure information is obtained from 71.5-MHz (^{29}Si) and 93.8-MHz (^{27}Al) NMR spectra recorded on a Brucker MSL360 spectrometer. Figure 3a shows the ^{29}Si spectrum recorded by using the magic angle spinning method (MAS) from the $x = 0.2$ compound fired at 800°C. The same spectra are observed for the two types of samples. The chemical shift position of −70 ppm (TMS used as a ^{29}Si chemical shift reference) is assigned to silicon in Q^0 tetrahedral environment, i.e., with four nonbridging oxygens per silicate tetrahedron. The low negative value of this Q^0 chemical shift agrees with ionic interactions between tetrahedra and neighboring ions (*8*).

However, in comparison with the pure lithium orthosilicate, the ^{29}Si spectrum exhibits some differences:

—As expected for a disordered solid solution, the ^{29}Si spectrum, for $x = 0.2$, is the envelope of the three NMR peaks (−62, −64, and −65 ppm) previously observed for $x = 0$ (*9*).

—The line is shifted towards high-field (−70 ppm). In fact, it is well-known that in

tetracoordinated silicon compounds, there is a linear correlation of the net charge q at the silicon and of the chemical shift in the -40, -120 ppm range (*10*). The lithium oxygen average length decreases when increasing x in the composition. Therefore, the effective oxygen electronegativity and the net charge q at the silicon increase, inducing a high-field shift.

Moreover, for all the compounds, no peak is observed at -75 ppm corresponding to silicium in a Q^1 (Al) tetrahedral environment, i.e., with three nonbridging oxygens and one Si–O–Al bridge per silicate tetrahedron. This confirms that all the aluminum atoms are localized on the silicon sites, as expected for the Li_4SiO_4–Li_5AlO_4 solid solution. No compound belongs to the Li_4SiO_4–$LiAlSiO_4$ solid solution.

Figure 3b shows the static ^{27}Al NMR spectra recorded at 93.8 MHZ for the two types of samples ($x = 0.2$) fired at 800°C. The spectra only exhibit a simple broaden symmetric line with a width at half intensity of about 6 kHz. Another ^{27}Al NMR investigation realized at 130.3 MHz leads to the same width, indicating that this latter is controlled by dipolar interactions. Frequency-dependent contributions, such as anisotropic chemical shift or second-order quadrupolar interactions are negligible and therefore Al atoms are localized on symmetric sites, as expected for a structure formed with isolated tetrahedra.

3. *Thermal Analysis*

X-ray diffraction and NMR data seem to indicate that A and B samples are made by a pure lithium orthosilicate-type phase. However, differential scanning calorimetry curves (DSC) (Fig. 4) clearly displayed some discrepancies in the chemical composition for the two types of samples. For the B sample, only one weakly intense peak is observed at 425°C (in fact, another peak is

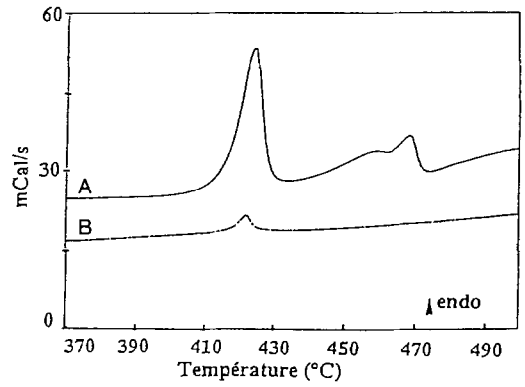

FIG. 4. Differential scanning calorimetry curves recorded from A- and B-type silicoaluminate samples, $x = 0.2$, fired at 800°C.

detected by differential thermal analysis at 718°C). In contrast, the curve recorded from the A sample exhibits three intense peaks at 420, 440, and 460°C. These data can be interpreted by using the $LiOH$–Li_2CO_3 phase diagram (*11*). The peak at 420°C is related to a polymorphic transition in the $7LiOH$–$2Li_2CO_3$ phase, the peak at 440°C corresponds to the melting of the eutectic composition, and the peak at 460°C results from the melting of the residual lithium hydroxide (Fig. 5).

For the B sample, the thermal analysis only shows the presence of traces of a Li_2CO_3-rich phase which resides at the surface. The B materials can be considered as pure aluminosilicates with Li_4SiO_4-type structure. Concerning the A sample, this technique clearly displays the presence of a LiOH-rich phase (a few wt%) which is protected against the carbonation and probably resides within grain boundary regions. The A materials appear as composite silicoaluminate and LiOH phases.

The presence of LiOH in the A materials directly derives from inhomogeneities in the sol–gel powder due to the use of a weakly reactive aluminum precursor. There is either an incomplete reaction of the initial

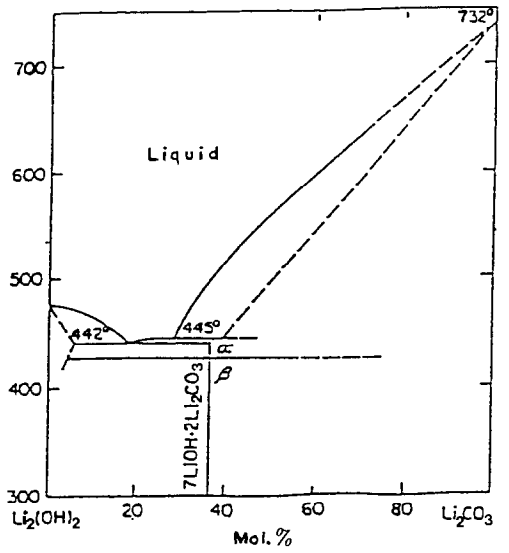

FIG. 5. Phase diagram in the $LiOH–Li_2CO_3$ system (from Ref. (*11*)).

LiOH or the formation of lithium-rich phases, such as Li_5AlO_4, which interacts with the air moisture. It has been previously shown (*12*) that LiOH easily appears in Li_5AlO_4 materials, via the reaction

$$Li_5AlO_4 + 2H_2O \rightarrow LiAlO_2 + 4LiOH.$$

Lithium Dynamics

1. Ionic Conductivity

Measurements of ac conductivity have been achieved according to the temperature (RT–400°C) on sintered disks (10 mm in diameter and 2 mm thick) by means of an HP 4192A impedance analyzer (input impedance of 10 MΩ) with frequencies ranging from 10 Hz to 13 MHz. Electrodes are provided by layers of gold evaporated onto both sides of the pellets. Measurements have been made in flowing dry nitrogen gas to avoid reaction of the lithium ceramic with the air moisture. Arrhenius plots of log σT vs $1/T$(°K), deduced from complex impedance plots for sol–gel lithium aluminosilicate ceramics are presented in Fig. 6.

For B-type materials, i.e., for pure lithium aluminosilicate compounds, the highest conductivity is obtained for the $x = 0.3$ compound, 5×10^{-4} S · cm^{-1} at 350°C, with an activation energy of 0.75 eV. Therefore, the ionic conductivity is only slightly increased, in comparison with the pure lithium orthosilicate ($x = 0$): 3×10^{-4} S · cm^{-1} at 350°C with an activation energy of about 1 eV. From these data (Table II), it is clear, in contrast with some previous studies (*5–7*), that upon substitution of the larger Al for Si and associated formation of charge compensating interstitial lithium ions, the ionic conductivity is not drastically modified. This suggests that a large part of the extra lithium ions is frozen around AlO_4^{5-} tetrahedra in the orthosilicate-type structure.

For A-type materials, i.e., for diphased materials, the ionic conductivity is largely increased compared to the pure lithium orthosilicate with small variations when changing the composition range (Table II). The highest value is 2×10^{-2} S · cm^{-1} at 350°C with an activation energy of about 0.55 eV. The magnitude of a such enhancement is greater at low temperature and amounts to some three orders of magnitude at 200°C. Owing to previous conductivity data (*5–7*) measured from conventional ceramics, that show results close to the values obtained for A compounds, it is clear that all these samples are two-phase systems formed of lithium hydroxide and lithium orthosilicate-type phases. In fact, the LiOH phase has not been observed in previous studies because its detection by X-ray diffraction implies concentration higher than 5 wt%.

Moreover, compared to B compounds, the enhancement of the ionic conductivity in A materials is directly related to the presence of LiOH, which presents poor ionic conductivity (5×10^{-7} S · cm^{-1} at 350°C)

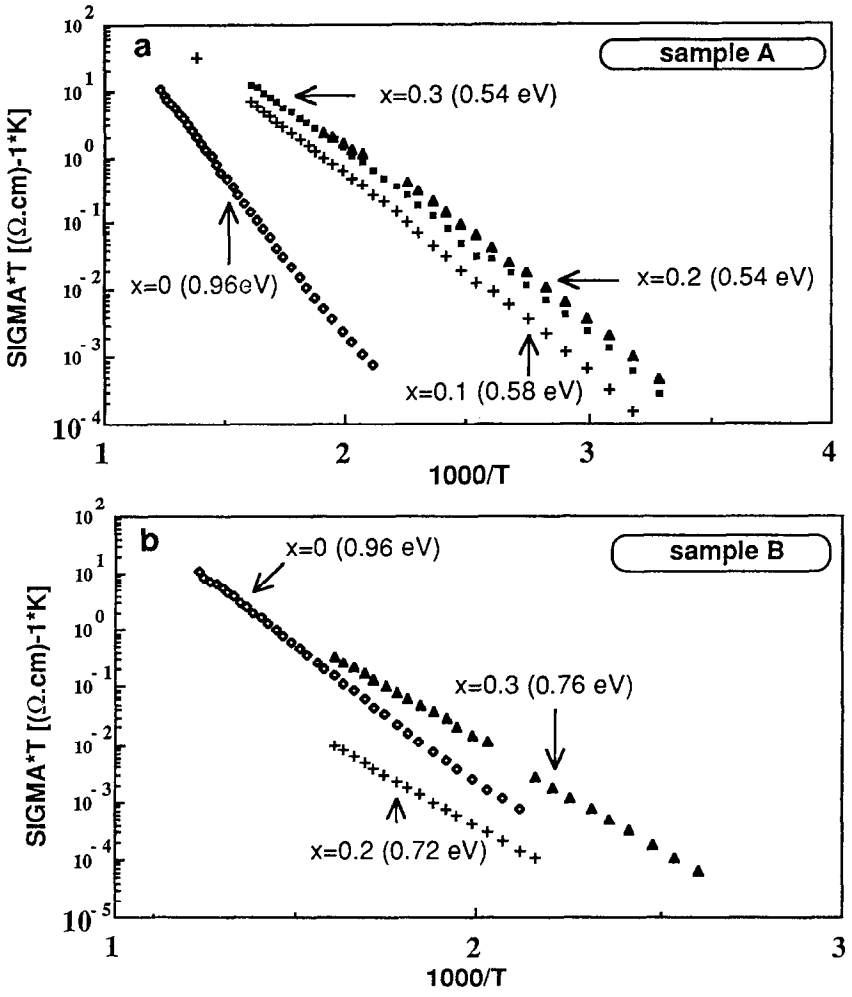

FIG. 6. Arrhenius plots of Log σT vs $1/T$(°K) for silicoaluminate samples in the Li_4SiO_4–Li_5AlO_4 solid solution, $Li_{4+x}Si_{1-x}Al_xO_4$ with $0 \leq x \leq 0.3$: (a) A-type samples, (b) B-type samples.

(*12, 13*). The same effect has been previously observed in Li_5AlO_4 materials containing the LiOH phase (*13*). In fact, it is well known that mixtures of solid ionic conductor such as βAgI, AgCI, or LiI with fine particles of an insulating material, such as Al_2O_3, can show a large increase in the ionic conductivity (*14, 15*). It is generally accepted that the enhancement is due to an increased conductivity along the interfacial region between inert particles and the conducting matrix. These kinds of materials have been called "composite or heterogeneous electrolytes." In the case of the A-type samples, the low value of the activation energy is consistent with the formation of a new kinetic path via a thin interphase layer along the interface itself or with an enhanced mobility along higher dimensional defects which have been formed as a result

TABLE II

IONIC CONDUCTIVITY AND ACTIVATION ENERGY FOR $Li_{4+x}Si_{1-x}Al_xO_4$ ($0.1 \leq x \leq 0.3$)

Sample	Composition (x)	Firing temperature (°C)	Activation energy (eV)	Conductivity ($S \cdot cm^{-1}$) 200°C	350°C
A	0.1	900	0.58	5.8×10^{-4}	1.1×10^{-2}
A	0.2	900	0.54	1.3×10^{-3}	2.0×10^{-2}
A	0.2	800	0.58	1.2×10^{-3}	2.0×10^{-2}
A	0.3	900	0.57	2.3×10^{-3}	1.5×10^{-2}
B	0.2	900	0.74	9.5×10^{-7}	6.3×10^{-5}
B	0.2	700	0.72	3.0×10^{-7}	1.6×10^{-5}
B	0.3	700	0.75	5.8×10^{-6}	5.3×10^{-4}

Note. B-type samples are monophase ceramics and A-type are diphased ceramics in which LiOH is expected to reside within grain boundary regions.

of the two-phase interaction (e.g., strain effect) (*16, 17*).

2. ^7Li Nuclear Magnetic Resonance

^7Li NMR spectra at room temperature. Figure 7a shows ^7Li signals observed at 24.8 MHz and at room temperature for the two types of samples A and B with the initial stoichiometry $Li_{4.2}Si_{0.8}Al_{0.2}O_4$. A very complex structure is observed with:

1. A central part composed of:
   —A sharp line with a width at half intensity of respectively 9 and 10.4 kHz for the A and B samples.
   —A broad line with a width of about 50 kHz for the two samples.
2. Satellite lines at ±370 kHz, in reference to the central line, for the two samples.

Figure 7b presents ^7Li spectra at 140 MHz and at room temperature for the two types of samples A and B. In a spectral range of 80 kHz, only one single line appears, with a width at half intensity of 13.3 and 13.8 kHz for the A and B samples, respectively. Therefore, the increase of the Larmor frequency (ω_0) leads to the disappearance of the broaden line (50 kHz width) observed at 24.8 MHz.

In the following, we suppose the existence of two populations of Li^+ ions. Taking as population I the lithium associated with the quadrupole satellite lines at $\omega_Q^{(1)} = 370$ kHz, the second order of quadrupole interactions $\omega_Q^{(2)}$, which contributes to the central linewidth for this population, can be approximately calculated according to the formula (*18*):

$$\omega_Q^{(2)} = \frac{25(\omega_Q^{(1)})^2}{48\omega_0}. \qquad (1)$$

This leads to $\omega_Q^{(2)} = 11.5$ kHz at $\omega_0 = 24.8$ MHz and only $\omega_Q^{(2)} = 2.0$ kHz at $\omega_0 = 140$ MHz.

At 24.8 MHz, the central line of population I is therefore included in the broad line localized in the central part of the spectra. This disappearance of the broad line at 140 MHz indicates:

—First, that the linewidth of population I is controlled by quadrupole interactions.

—Second, that at $\omega_0 = 24.8$ MHz, the broad linewidth of 50 kHz is a mixture of the central line of population I and of the quadrupole satellites for an other population (denoted II).

If we calculate $\omega_Q^{(2)}$ for this population II,

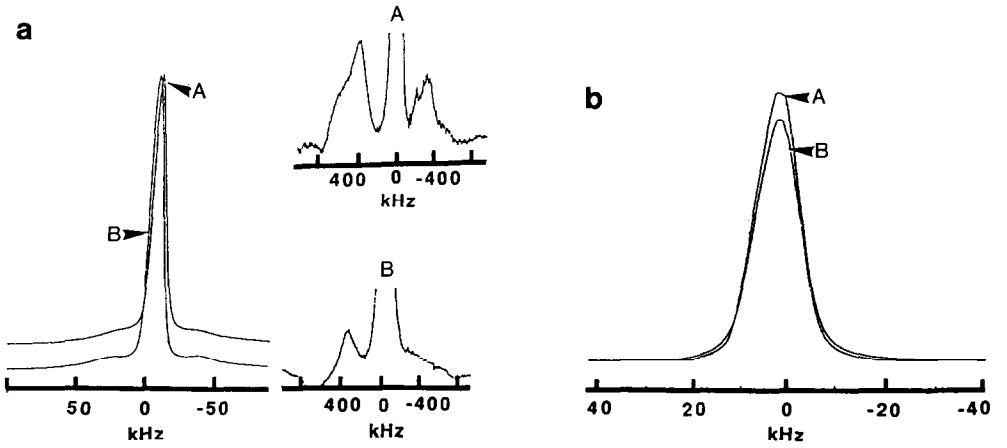

FIG. 7. ^{7}Li NMR spectra at room temperature for the A- and B-type silicoaluminate samples ($x = 0.2$): (a) at 24.8 MHz with detailed spectra showing quadrupolar satellite lines, (b) at 140 MHz.

by using Formula (1), we obtain 52 and 9 Hz at 24.8 and 140 MHz, respectively. Therefore, the central line of this population, which is the sharp line observed at 24.8 MHz, is mainly controlled by static dipolar interactions.

These dipolar interactions (10 kHz) are independent of ω_0. Consequently, the linewidths of 13.3 and 13.8 kHz for A and B samples at $\omega_0 = 140$ MHz are due to a mixture of two interactions: static dipolar interactions of 9 or 10.4 kHz for population II and second-order quadrupolar interactions of approximately 2.0 kHz for population I. The complementary contribution (about 2 kHz) can be assigned to the transverse relaxation.

A surprising fact is the disappearance, at 140 MHz, of the quadrupole satellite lines of population II (±25 kHz). However, for a $\frac{3}{2}$ spin, the frequency dependence of the transverse quadrupolar relaxation is different for the central line and for satellites (*19*). A similar effect, concerning the temperature dependence, is reported below.

To summarize, for the two types of samples at room temperature, NMR data can be interpreted by the presence of two stationary lithium populations. The first localized into distorded sites (population I) and the second into undistorted sites (population II).

^{7}Li NMR spectra at 440°C. Figure 8 shows ^{7}Li spectra at 24.8 MHz and 440°C for both samples. In comparison with the spectra recorded at RT, the quadrupolar satellite lines (±370 kHz) of population I are not significantly modified. In contrast, a dissymmetric central line with a width at half intensity of 2.5 kHz and satellite lines at ±5 kHz are observed in the central part of the

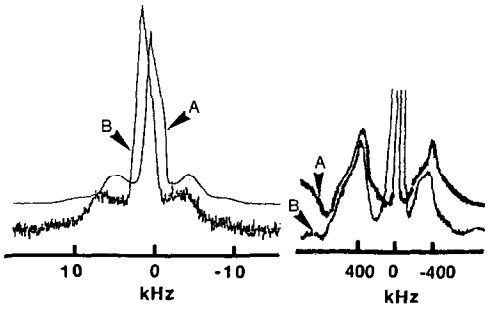

FIG. 8. ^{7}Li NMR spectra at 24.8 MHz and at 440°C, with detailed quadrupole satellite lines, for the A- and B-type silicoaluminate samples ($x = 0.2$).

spectra. Moreover, the position of the satellite lines (±5 kHz) is the same for another Larmor frequency (14.2 MHz).

These data confirm again the presence of two lithium populations:

—The satellite lines at ±5 kHz are due to the first-order quadrupole interactions for population II. The corresponding value of $\omega_Q^{(2)}$ is only 2 Hz for $\omega_0 = 24.8$ MHz. Therefore, the reduction of the central line of the population II, from 10 kHz at room temperature to 2.5 kHz at 440°C, is related to the motional averaging of dipolar interactions, this population being mobile at such temperature.

—The quadrupolar satellite lines at ±370 kHz are always characteristic of population I, which remains fixed at 440°C. The width of the corresponding central line, controlled by the second-order quadrupole interactions, has been previously evaluated to 11.5 kHz for $\omega_0 = 24.8$ MHz. This value is higher than the experimental one (less than 2.5 kHz), due to the motion of the lithium II, which modifies differently the first- and the second-order quadrupolar interactions for population I. This comes from the effective Hamiltonian, which is different, in the rotating frame, for first- and second-order quadrupolar interactions (*20*).

At 440°C, the analysis of the ^{7}Li NMR spectra displays the existence of two lithium populations for both types of samples: the first one is fixed and localized into distorted sites (population I) and the second is mobile and localized into undistorted sites (population II).

Temperature dependence of the ^{7}Li NMR spectra. Figure 9 presents the temperature dependence of the central part of the Li spectrum observed at 24.8 MHz for the A sample. The width of the central line of population II, controlled by static dipolar interactions at room temperature (9 kHz), is reduced to 7 kHz by increasing the temperature up to 100°C. The narrowing of this line, corresponding to the motional averaging of dipolar interactions, is due to the onset of the lithium motion which takes place between 50 and 100°C.

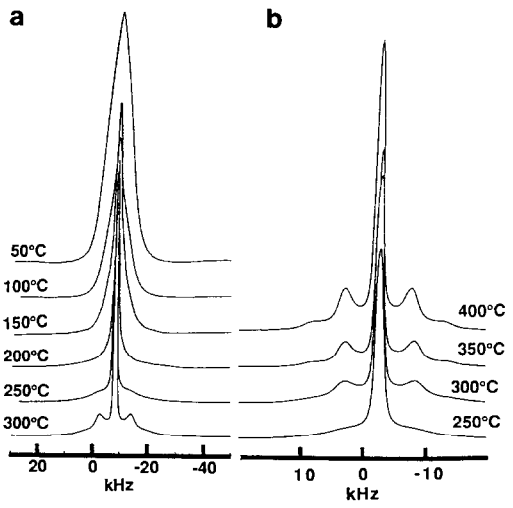

FIG. 9. Temperature dependence of the ^{7}Li NMR spectra at 24.8 MHz, for the A-type sample ($x = 0.2$): (a) from 50 to 300°C, (b) from 250 to 400°C.

Another interesting fact corresponds to the temperature dependence of the quadrupolar satellite lines of this population II. Below 50°C, the satellite lines at ±25 kHz are hardly visible and disappear at 100°C (Fig. 9a). Above 250°C (Fig. 9b), two satellite lines appear at ±5 kHz, due to the residual time averaging of quadrupole interactions by anisotropic ionic motion. Between 100 and 200°C, the inverse of the characteristic motional time (τ_c) becomes of the same order of magnitude as the quadrupole interactions ($\Delta_Q = 50$ kHz) seen by lithium II, i.e., $\tau_c = 1/(2\pi\Delta_Q) = 6.4 \times 10^{-6}$ sec. In this temperature range, quadrupolar interactions evolve from a static state to a fluctuating one with an amplitude of 40 kHz. The relaxation process is controlled by these quadrupolar interactions. At 200°C, the transverse relaxation time, i.e., the homoge-

neous part of the satellite linewidth (Δ) can be calculated from Δ (Hz) = $2\pi(\omega_Q)^2\tau_c$, with ω_Q (in kHz) = 40 kHz, leading to Δ = 64 kHz.

This value is very high, in comparison with the residual quadrupole interactions (5 kHz). Consequently, the quadrupolar ^{7}Li NMR spectra are only well resolved at higher temperature, where the characteristic time and therefore the homogeneous width are sufficiently reduced. Concerning the central line of population II, the homogeneous width is controlled, at high temperature, by the inverse of the longitudinal relaxation time. This confirms that, for a $\frac{3}{2}$ spin, the temperature dependence of the transverse relaxation time is different for satellites and central line (*19*).

In conclusion, we have shown that ^{7}Li NMR spectra are very similar for the two types of samples. Upon substitution of Al for Si and introduction of extra lithium, a dissymmetry of charge is induced in the skeleton. AlO_4^{5-} anionic clusters are equivalent to negative charges in the tetrahedral sublattice. Therefore, the attractive electrostatic interaction leads to the freezing of a part of the lithium ions. This gives two different lithium populations:

—The first population weakly interacts with AlO_4^{5-} and becomes mobile above 50°C.

—The second population highly interacts with AlO_4^{5-} and remains fixed at high temperature.

The difference of mobility is sufficiently important to explain the temperature variation of the NMR spectra of both samples.

3. *^{7}Li Longitudinal Relaxation Times*

The spin-lattice relaxation times, T_1, of ^{7}Li nuclei, are measured between room temperature and 600°C, at 24.8 MHz, by using the inversion recovery method. Figure 10 shows the temperature dependence of the longitudinal relaxation rate $1/T_1$ for the two types of samples. The observation of a maximum of $1/T_1$ is characteristic of a thermally activated motion. Close to the maximum, curves exhibit an "M" shape which is enhanced for the A sample. Moreover, for this sample, at low temperature, precise and reproducible measurements of the T_1 are difficult. In fact, for a $\frac{3}{2}$ spin system, the nuclear magnetization does not return to equilibrium with a single characteristic time, in the temperature range in which the correlation time, characteristic of the motion, is greater than $1/\omega_0$.

On the low temperature side of the relaxation data, i.e., in the temperature ranges of 25–253°C and 25–352°C for A and B samples, respectively, the apparent slopes lead to the same activation energy of 0.23 eV. A similar value has been previously reported for the pure lithium orthosilicate and for compositions in the Li_4SiO_4–Li_3PO_4 solid solution (*21*). The local motion relaxation is therefore identical for all these compounds and lithium ions are constrained to jump over this potential barrier to contribute to the motion. This activation energy can be attributed to the formation of Frenkel defects in the Li_4SiO_4-type structure.

On the high temperature side of the relaxation data, i.e., in the temperature ranges of 352–560°C and 416–560°C for A and B samples, respectively, the apparent slopes are relatively close to the ones observed in the low temperature ranges. The activation energies are respectively 0.28 and 0.24 eV for A and B samples (note that the points at 596°C are excluded of the fit for the two samples). Therefore, the behavior of these materials can be approximately described by using the well known BPP model (*22*). In this model, a simple form of the correlation function $G(\tau)$ is used: $G(\tau) \propto \exp(-t/\tau)$, where τ is the correlation time of the fluctuations. Quite often τ is described by an Arrhenius law, $\tau = \tau_0 \exp(E/kT)$, and is identi-

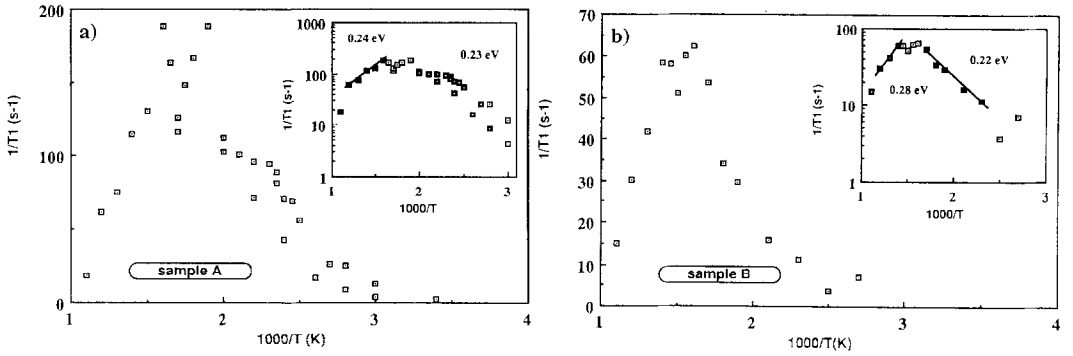

FIG. 10. Longitudinal ^{7}Li relaxation rate versus the inverse of the temperature (semilogarithmic curve in the insert) at 24.8 MHz for silicoaluminate ceramics (x = 0.2): (a) A-type samples, (b) B-type samples.

fied with a characteristic time of the motion. This could be the residence time of an ion in a given site before the jump. Then, E is the activation energy of this process and $1/\tau_0$ is the "attempt frequency" at large temperature. The simple BPP expression predicts the same activation energy on either side of the T_1 minimum, as observed for the two silicoaluminate samples. In the high temperature regime, the behavior of these samples is then consistent with the existence of uncorrelated jumps between equivalent sites. Nevertheless, this analysis implies that a long range motion takes place for lithium ions and, at 560°C, the characteristic time of the motion is only three times lower than the inverse of the Larmor frequency ($1/\omega_0$). This small variation of the characteristic time, due to the low activation energy of the process, prevents direct connection of relaxation with conductivity data. Moreover, it is possible that the high values of T_1, measured for the two samples at 596°C and which did not follow the previous activated laws, indicate a change in the microscopic Li^+ dynamics.

In the intermediary temperature ranges, the two maxima, at 253 and 352°C for the A sample and at 352 and 416°C for the B sample, as well as the "M" shape of the ^{7}Li relaxation curves, can be interpreted in terms of two lithium populations (mobile and stationary ions).

Taking τ_{ma} and τ_{mb} for the characteristic times of the mobile ions in A and B samples, and τ_{fa} and τ_{fb} for the characteristic times of the fixed ions in A and B samples, the attempt frequencies can be deduced from the relation $\omega_0\tau = 1$ valid around the maxima. This gives:

$1/\tau^0_{ma} = 2.5 \times 10^{10}$ Hz and

$1/\tau^0_{fa} = 1.1 \times 10^{10}$ Hz for the A compound,

$1/\tau^0_{mb} = 10^{10}$ Hz and $1/\tau^0_{fb} = 5.8 \times 10^9$ Hz for the B compound.

For the two samples, the ratio τ^0_f/τ^0_m is close to two, corresponding to the effects of change of reference in the theoretical study of the ionic dynamics. In fact, for species with the same mass, the diffusion coefficient is twofold in a mobile reference system (*23*). In addition, the existence of a single ^{7}Li relaxation rate, above 200°C, shows that the nuclear magnetization of the two species is always in thermal equilibrium, and that the ^{7}Li longitudinal relaxation measure-

ments reach it the fastest. The "M" shape of the curves is therefore directly related to the existence of two lithium populations, one with fixed ions and one with mobile ions, and to the change of the reference system.

A first significant difference between A and B samples is that the relaxation rate maximum is higher for the A sample than for the B sample (190 sec^{-1} instead of 60 sec^{-1}). As previously noted in the ^7Li spectral analysis, the ^7Li relaxation is controlled by quadrupole interaction fluctuations with intensity about 40 kHz. Assuming an exponential correlation function, the value of the maximum of the relaxation rate can be deduced from the following formula: $(1/T_1)_{max} = \varepsilon^2/\omega_0$, where ε is the fluctuating interaction. This leads to 65 sec^{-1}, a value very close to the experimental value for the B material. In contrast, a higher value is observed for *A* (190 sec^{-1}), associated with quadrupole interactions of 69 kHz. Consequently, the ^7Li motion generates quadrupolar fluctuations with a lower intensity in the B sample. This suggests that the fluctuations of the electric field gradient, caused by lithium diffusion, are more screened in the B compound, corresponding to higher apparent polarizability of the tetrahedra sublattice.

Other important differences between the relaxation curves are that the splaying is more important and that the $1/T_1$ peak moves to higher temperatures for the B curve. In fact, we have seen that the values of τ^0_{ma} and τ^0_{fa} are respectively two times lower that τ^0_{mb} and τ^0_{fb}. This indicates that the motion is slower in the B compound, which can also be interpreted as a difference in the apparent polarizability of the tetrahedra in the two materials. The skeleton is formed of negative tetrahedra cages which are opposed to the positive charge motion and the screening of the mobile charge appears more efficient in the B sample.

Conclusion

Lithium aluminate-doped lithium orthosilicate powders have been prepared from the alkoxide–hydroxide sol–gel route. By using reactive aluminum alkoxide, the sintering of the powders has led to dense B-type monophase ceramics at low temperature (700–800°C). In contrast, by using less reactive polymerized aluminum alkoxide, A-type diphase ceramics have been prepared. X-ray diffraction and ^{29}Si MAS–NMR techniques showed that the lithium silicoaluminate phases belong to the Li_4SiO_4–Li_5AlO_4 solid solution and exhibit the Li_4SiO_4-type structure: $Li_{4+x}Si_{1-x}Al_xO_4$ ($0 \leq x \leq 0.3$). In the A-type materials, the thermal analysis displays a few LiOH in weight%, coexisting with the silicoaluminate phase, which results from chemical inhomogeneities in the initial sol–gel powder.

^7Li NMR has shown very similar spectra for the two types of samples (A and B), suggesting that the LiOH phase is mainly localized within grain boundary regions in the A-type materials. The ^7Li spectra have been interpreted in terms of two lithium populations. The first one, localized into distorted sites, is considered fixed in the 25–600°C temperature range and the second, localized into undistorted sites, is considered mobile above 50°C. The presence of two lithium populations has been directly related to the charge dissymmetry in the tetrahedra sublattice, which led to the freezing of a part of the lithium ions by attractive interactions with AlO_4^{5-} tetrahedra.

Compared to the pure Li_4SiO_4, the ionic conductivity is slightly increased in silicoaluminate monophase ceramics (B-type). In disagreement with the results of Shannon *et al.* (*5*) and Jackowska *et al.* (*7*), we have shown that the introduction of extra lithium in the Li_4SiO_4-type structure did not drastically enhance the lithium transport properties. However, the conductivity has increased by two orders of magnitude at 350°C

in A-type materials ($x = 0.2$ and $x = 0.3$) and the highest value (4×10^{-2} S · cm^{-1} at 350°C) is close to the one previously reported by Shannon *et al.* (*5*) for conventional ceramics. This clearly shows that:

—High conductivity in lithium silicoaluminate materials requires the presence of an inert phase, such as LiOH, coexisting with the Li_4SiO_4-type phase. The enhancement of the ionic conductivity can then be interpreted as the formation of a new kinetic path, via a thin interphase layer along the interface.

—High conductivity values, previously reported for silicoaluminate compositions, are due to chemical inhomogeneities (presence of LiOH) in samples prepared by the conventional ceramic processing.

Concerning ^{7}Li longitudinal relaxation measurements, the differences observed between A- and B-type materials, i.e., time and temperature shifts of the curves, can be interpreted from the variation of the apparent polarizability of the tetrahedra skeleton. The lower polarizability of the A sample can be directly related to the presence of lithium hydroxide in this material. The localization of a small part of this second phase inside the grains of the aluminosilicate ceramic generates structural disorder and prevents the tetrahedra deformation, decreasing the screening of the mobile charge. However, the difference of the lithium mobility is relatively weak for these compounds and cannot explain the drastic variations of conductivity. Therefore this is a further confirmation that the enhancement of the conductivity in the A sample is due to a new kinetic path along the interface between the two phases.

References

1. W. Weppner, *in* "Fast Ionic Transport in Solids", (J. B. Bates and G. C. Farrington Eds.) p. 3 North Holland (1981).
2. W. Breitung, H. Elbel, J. Lebkücher, G. Schumacher, and H. Werle, *J. Nucl. Mater.* **155–157,** 507 (1988).
3. D. Tranqui, R. D., Shannon, and H.-Y. Chen, *Acta Crystallogr. B* **35,** 2479 (1979).
4. Y-W. Hu, I. D. Raistrick, and R. A. Huggins, *Mater. Res. Bull.* **11,** 1227 (1976).
5. R. D. Shannon, B. E. Taylor, A. D. English, and T. Berzins, *Electrochim. Acta* **22,** 783 (1977).
6. Y-W. Hu, I. D., Raistrick, and R. A. Huggins, *J. Electrochem. Soc.* **124,** 1240 (1977).
7. K. Jackowska and A. R. West, *J. Mater. Sci.* **18,** 2380 (1983).
8. M. Smaihi, J. P. Boilot, P. Bergez, and J. M. Boncoeur, *in* "Advances in Ceramics" (G. W. Hollenberg and I. J. Hastings, Eds.), Vol. 27, p. 23, Amer. Ceram. Soc. Colombus, OH (1990).
9. M. Smaihi, D. Petit, J. P. Boilot, F. M. Botter, J. Mougin, and J. M. Boncoeur, "The Proceedings of the 16th Symposium on Fusion Technology," London, U.K., September 3–7, (1990).
10. G. Engelhard and D. Michel, "High Resolution Solid-State NMR of Silicates and Zeolites," Wiley, New York (1987).
11. O. G. Perfil'eva, *Russ. J. Inorg. Chem.* **9,** 1406 (1964).
12. R. T. Johnson, R. M. Biefeld, and J. D. Keck, *Mater. Res. Bull.* **12,** 577 (1977).
13. R. T. Johnson, J. R. and R. M. Biefeld, *in* "Fast Ion Transport in Solids" (P. Vashishta, J. N. Mundy, and G. K. Shenoy, Eds.), p. 457, North-Holland, Amsterdam (1979).
14. C. C. Liang, *J. Electrochem. Soc.* **120,** 1289 (1973).
15. K. Shahi and J. B. Wagner, *J. Electrochem. Soc.* **128,** 6 (1981) and *J. Solid State Chem.* **42,** 107 (1982).
16. J. Maier, *in* "Superionic Solids and Solid Electrolytes," p. 137, Materials Science Series, Academic Press (1989).
17. H. E. Roman, *Phase Transitions* **24–26,** 435 (1990).
18. M. H. Cohen and F. Reif, *Solid State Physics* **5,** 339 (1957).
19. D. Petit and J. P. Korb, *Phys. Rev. B* **37,** 5761 (1988).
20. R. R. Ernst, G. Bodenhausen, and A. Wokaun, Principles of Nuclear Magnetic Resonance in One and Two Dimensions, Ch. 3, Oxford University Press (1987).
21. M. Smaihi, D. Petit, F. Gourbilleau, F. Chaput, and J. P. Boilot, submitted for publication.
22. N. Bloembergen, E. M. Purcell, and R. V. Pound, *Phys Rev.* **73,** 679 (1948).
23. A. Abragam, "The Principles of Nuclear Magnetism," Ch. 8 p. 301, Oxford University Press (1961).